Chapter 12

Palladium (II) Oxide Nanostructures as Promising Materials for Gas Sensors

Alexander M. Samoylov, Stanislav V. Ryabtsev, Vasily N. Popov and Petre Badica

Additional information is available at the end of the chapter

http://dx.doi.org/10.5772/intechopen.72323

Abstract

One of the most important environment monitoring problems is the detection of oxidizing gases in the ambient air. Negative impact of noxious oxidizing gases (ozone and nitrogen oxides) on human health, sensitive vegetation, and ecosystems is very serious. For this reason, palladium (II) oxide nanostructures have been employed for oxidizing gas detection. Thin and ultrathin films of palladium (II) oxide were prepared by thermal oxidation at dry oxygen of previously formed pure palladium layers on polished poly-Al_2O_3, SiO_2/Si (100), optical quality quartz, and amorphous carbon/KCl substrates. At ozone and nitrogen dioxide detection, PdO films prepared by oxidation at T = 870 K have demonstrated good values of sensitivity, signal stability, operation speed, and reproducibility of sensor response. In comparison with other materials, palladium (II) oxide thin and ultrathin films have some advantages at gas sensor fabrication. Firstly, for oxidizing gas detection, PdO films with *p*-type conductivity are more perspective than the material with *n*-type conductivity. Secondly, at ambient conditions, palladium (II) oxide is insoluble in water and does not react with it. These facts are favorable for the fabrication of gas detectors because they make possible to minimize the air humidity influence on PdO sensor response values. Thirdly, the synthesis procedure of PdO films is rather simple and is compatible with planar processes of microelectronic industry.

Keywords: palladium (II) oxide, nanostructure, gas sensor, ozone, nitrogen dioxide

1. Introduction

Nowadays, the detection of oxidizing gases in the ambient air is one of the most important environment monitoring problems for industrialized countries. During the last 25 years, the

steady increase in concentration of nitrogen dioxide and tropospheric (low level) ozone is observed. As it is known, three out of six common air pollutants (also called "criteria pollutants") are oxidizing gases: sulfur dioxide, nitrogen oxides, and tropospheric ozone [1, 2]. One part of ecologists is sure that increase in the content of low-level ozone in atmospheric air is caused mainly by an intensification of industrial production, motor and air transport. Undoubtedly, ozone gas is applied in many fields such as food, pharmaceutical, textile, and chemical industries, water treatment, and purification of gases. However, there is an opinion that emergence of tropospheric ozone in ambient air is a consequence of the "greenhouse" effect [3].

Under sunlight, the interaction of ozone, nitrogen oxides, and volatile hydrocarbons can produce many toxic organic compounds (**Figure 1**). By the action of sunlight, oxygen atoms freed from nitrogen dioxide attack oxygen molecules to make ozone. Nitrogen oxide can combine with ozone to reform nitrogen dioxide, and the cycle repeats.

Moreover, at interaction with ozone, the ultraviolet component of sunlight leads to the formation of excess quantity of the reactive oxygen species (ROS): oxygen ions, free radicals, and peroxides. In living bodies, even the trace amounts of ROC can provoke an oxidative stress. For human, the oxidative stress is a reason for atherosclerosis, hypertension, Alzheimer's disease, diabetes, and geromorphism [4–9]. The negative impact on human health of an aspiration of noxious oxidizing gases (ozone and nitrogen oxides) is more serious, particularly for children, the elderly, and people who suffer from lung diseases [1, 2]. Nitrogen oxides and tropospheric ozone can also have harmful effects on sensitive vegetation and ecosystems [10–13].

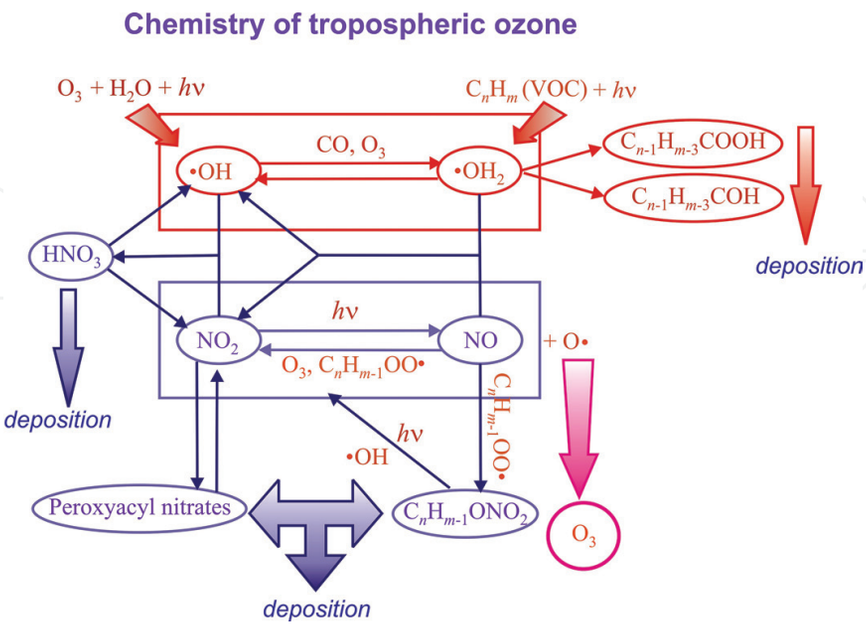

Figure 1. The chemical reactions of tropospheric ozone under sunlight.

For these reasons, various types of the binary, ternary and quaternary metal-oxide semiconductors have been widely applied for oxidizing gas detection. In most cases, for this purpose, the *n*-type semiconductors such as SnO_2 [14–20], ZnO [21–26], WO_3 [27–32], In_2O_3 [33, 34], and TiO_2 [35] are used traditionally. In recent years, the search of the materials, which would be capable to lower the detection limit of oxidizing gases, became more active.

The study of palladium (II) oxide nanostructures as materials for gas sensor fabrication was started only since 2014. The assumption to use palladium (II) oxide, which is a *p*-type semiconductor with the energy band gap $\Delta E_g = 2.2–2.7$ eV [36–38], as the material for the detection of toxic and highly inflammable gas in ambient air has not been accidental for some reasons [39, 40]. Firstly, for a long time, palladium and its compounds in (+2) oxidation state were exploited as very effective catalysts for oxidation reactions of hydrocarbons, including automobile catalytic converters and the catalytic combustion of methane in advanced gas turbines. In catalytic converters, the key processes are the complete oxidation of any hydrocarbon in the exhaust gas stream, the simultaneous oxidation of carbon monoxide, and reduction of nitrogen oxides. Secondly, due to the extremely high catalytic activity, palladium and palladium (II) oxide were applied as additives to improve gas-sensing performance of tin dioxide SnO_2 to a wide range of gases [41–43]. Thirdly, the opinion that long recovery process and high stability could be referred to the main disadvantages of the oxidizing gas sensors based on tin dioxide has been expressed earlier [44, 45]. Fourthly, the metal oxide semiconductors with *p*-type conductivity are more perspective for oxidizing gas detection than the materials with *n*-type conductivity. In this case, the chemical adsorption of oxidizing gas molecule on *p*-type semiconductors surface leads to decrease in the sensor resistance that has simplified the detection process [35, 36]. Thus, at oxidizing gas detection, palladium (II) oxide nanostructures should demonstrate the increase in sensor response value in comparison with the traditional *n*-type conductivity materials using for the same purpose.

2. Fabrication of palladium (II) oxide nanostructures

Initially, the sensing properties to oxidizing gases of palladium (II) oxide nanostructures were tested on ultrathin and thin films at detection of ozone and nitrogen dioxide [46, 47]. The procedure of PdO thin and ultrathin films synthesis was realized by two stages. First, the initial palladium films (thickness 5–30 nm) were formed by thermal sublimation of palladium foil (purity is 99.99%) in high vacuum chamber evacuated to 5×10^{-7} Torr using a turbo molecular pump. In vacuum chamber, the condensation of Pd metal vapors was performed on different substrates: SiO_2/Si (100), Si (100), optical quality quartz, and KCl (100) with buffer layer of amorphous carbon (**Figure 2**). The values of tungsten heater temperature in order to fabricate initial palladium films with average rate within interval 0.01–0.016 nm per second were determined as a result of Pd films cross-sections by high-resolution scanning and transmission electron microscopy (HR STEM) study.

The substructure of initial palladium layers was studied by an X-ray analysis and the HEED method. As it is shown in **Figure 3a** and **3b**, the initial Pd films were polycrystalline and

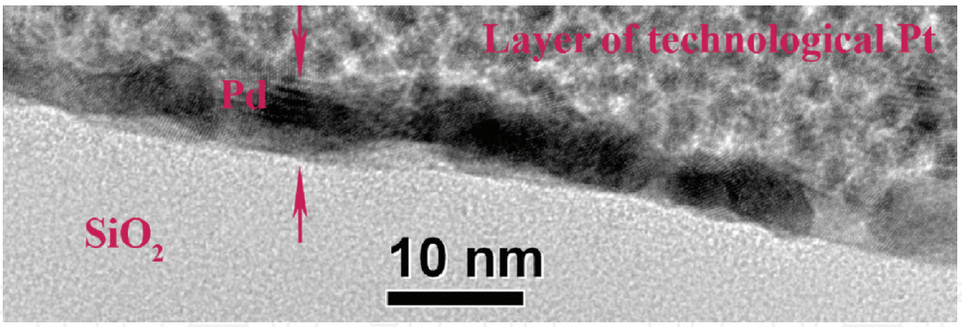

Figure 2. High-resolution TEM image of Pd/SiO_2/Si (100) heterostructure cross-section prepared by focused ion beam (FIB) technique.

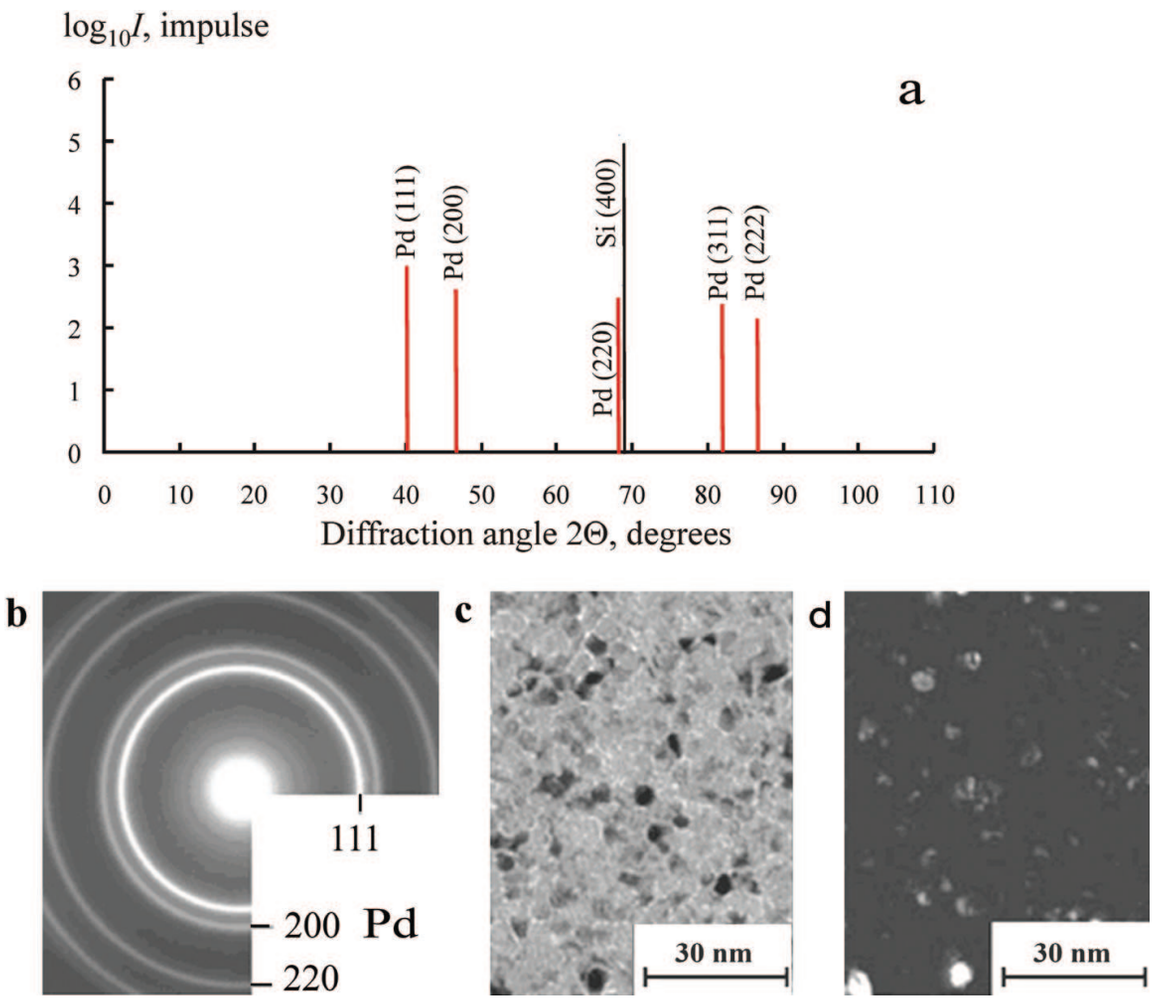

Figure 3. Experimental results of initial Pd films (thickness ~10 nm) crystal structure study: (a) XRD patterns of Pd film deposited on Si (100) substrate; (b) HEED patterns of Pd film deposited on amorphous carbon/KCl substrate; (c) bright-field TEM image of Pd film deposited on amorphous carbon/KCl substrate; (d) dark-field TEM image of Pd film deposited on amorphous carbon/KCl substrate.

highly dispersive with random orientation of grains irrespective of the substrate nature (SiO_2/Si (100), optical quality quartz, and amorphous carbon/KCl). The analysis of *bright-field* (**Figure 3c**) *and dark-field* (**Figure 3d**) TEM images proves that palladium crystalline grains form a continuous coating without an axial texture with very low density of micropores. On bright-field image, the light contrast (**Figure 3c**) testifies to the decrease of film thickness at grain borders [48].

Prepared Pd nanostructures on different substrates were annealed at dry oxygen atmosphere for 1 h for layers with thickness 5–15 nm and for 2 h for layers with thickness 30 ± 5 nm at temperatures T_{ox} = 510, 570, 670, 770, 870, and 1070 K. The dehumidification of oxygen at pressure 120–130 kPa (1.2–1.3 Bar) was carried out by gas flow passage through gas bubbler with concentrated sulfuric acid and further through silica tube full of ground zeolite [48].

3. Phase composition and crystal structure of palladium (II) oxide nanostructures

X-ray diffraction (XRD) patterns of samples prepared by oxidation of Pd films on SiO_2/Si (100) wafers at dry oxygen atmosphere at T_{ox} = 510, 570, 770, 870, and 970 K are shown in **Figure 4**.

It is necessary to note that in **Figure 4**, the values of XRD reflex intensities are presented in a logarithmic scale because the intensity of Si (400) peak practically exceeds the intensity of palladium and palladium (II) oxide peaks by two orders of magnitude owing to a small thickness of the prepared films. The comparison of the as-grown Pd films XRD patterns with XRD patterns of Pd film after the annealing at T_{ox} = 510 K (**Figure 4a**) did not reveal any quality changes. The increase in intensities of palladium reflexes was found only.

Thus, it has been established that the annealing of Pd layers at T_{ox} < 570 K (**Figure 4a**) did not result in the change of their phase constitution. The annealing at T_{ox} = 570 K resulted in the formation of two phase films (**Figure 4b**). XRD patterns have shown the presence of Pd with PdO simultaneously.

According to XRD results, the rise of the oxidation temperature up to T_{ox} = 770 K and T_{ox} = 870 K led to the formation of the homogenous polycrystalline PdO films. It has been determined (**Figure 4c** and **4d**) that palladium (II) oxide films were characterized by tetragonal crystal lattice (space group $P4_2/mmc$ and PtS structure type). XRD patterns show (**Figure 4c–4e**) that the peaks became sharper and higher with the oxidizing temperature increasing from T_{ox} = 770 K up to T_{ox} = 970 K. Moreover, the peaks of palladium (II) oxide prepared by oxidation at T_{ox} = 970 K are much sharper and higher than those for films oxidized at T_{ox} = 870 K. This fact can be interpreted as one of the evidences of the crystalline perfection enhancement of palladium (II) oxide films and the grain size enlargement with the increase in the oxidation temperature.

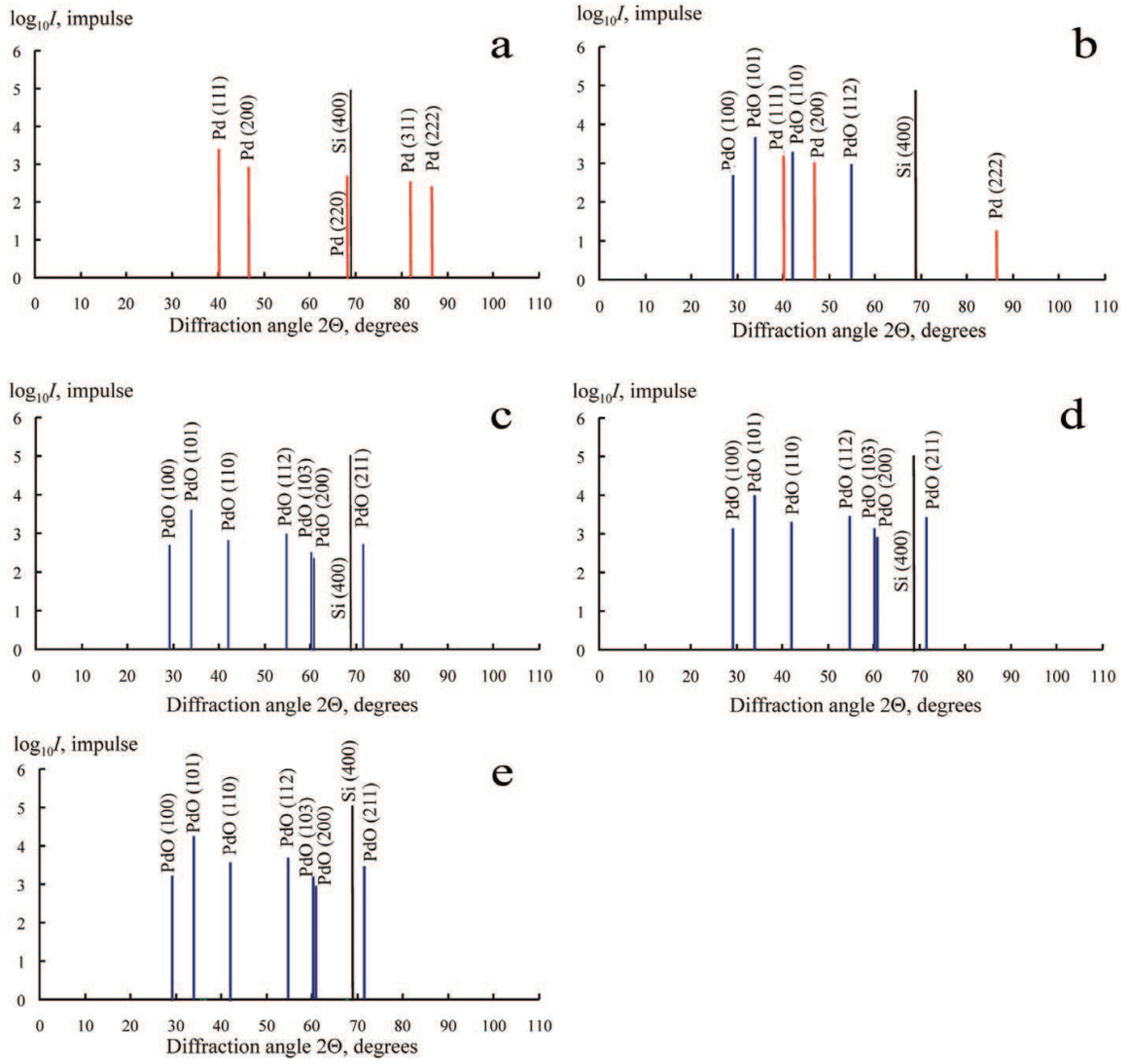

Figure 4. X-ray diffraction patterns of palladium film deposited on SiO_2/Si (100) substrate after oxidation in dry oxygen at different temperatures: *a*—T_{ox} = 510 K; *b*—T_{ox} = 570 K; *c*—T_{ox} = 770 K; *d*—T_{ox} = 870 K; and *e*—T_{ox} = 970 K.

High energy electron diffraction (HEED) technique was used as an alternative method to study PdO film phase composition (**Figure 5**).

Table 1 compares the results of X-ray analysis (layers on SiO_2/Si substrates), the HEED method (layers on optical quartz and Al_2O_3 substrates), and TEM micro diffraction (layers on amorphous carbon/KCl). An examination of the data presented in **Table 1** shows that the X-ray analysis, HEED method, and TEM micro diffraction gave the identical results for the films oxidized at temperatures T_{ox} = 510, 570, 770, 870, and 970 K. The results of these two methods confirm that: (1) the annealing of Pd films at T_{ox} = 510 K does not induce the changes in their phase composition; (2) after annealing of Pd films at the T_{ox} = 570 K, the partial oxidation takes place and gives two phase samples – a mixture of Pd and PdO; and (3) after the annealing of palladium layers at T_{ox} = 770–970 K, the total oxidation gives homogeneous PdO films [48].

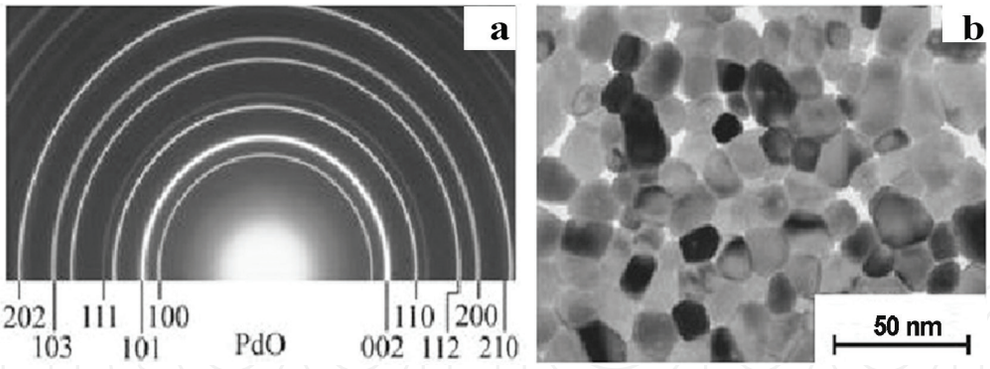

Figure 5. HEED patterns (*a*) and bright-field TEM image (*b*) of PdO film after oxidation at T_{ox} = 870 K.

Oxidation temperature T_{ox}, K	Phase composition		
	X-ray analysis	HEED	TEM microdiffraction
510	Pd	Pd	Pd
570	Pd + PdO	Pd + PdO	Pd + PdO
670	—	PdO	—
770	PdO	PdO	PdO
870	PdO	PdO	PdO
970	PdO	PdO	PdO

Table 1. Results of phase composition study of Pd films after oxidation at ***T*** = 500–970 K.

4. Electrical properties of palladium (II) oxide nanostructures

The type of conductivity of PdO films synthesized at T_{ox} = 770–970 K was determined by the Seebeck effect study and by calculation of the electromotive force E_{emf} values:

$$E_{emf} = -S \nabla T, \quad (1)$$

where S is thermo-power (Seebeck coefficient), and ∇T is the temperature gradient. Copper-constantan thermocouples have been used to measure a temperature difference.

Experimental values of E_{emf} have proved the *p*-type conductivity for all homogeneous palladium (II) oxide films (**Figure 6**). The fact of *p*-type conductivity of PdO bulk samples was reported in the previous publications [36, 37]. The values of thermo power (Seebeck coefficient) S have been calculated using the Eq. (1). Depending on thickness of palladium oxide films and oxidation temperature, the Seebeck coefficient values changed within the limits from +120 to +220 μV/K. The relative error at thermo-power measurement did not exceed 7%.

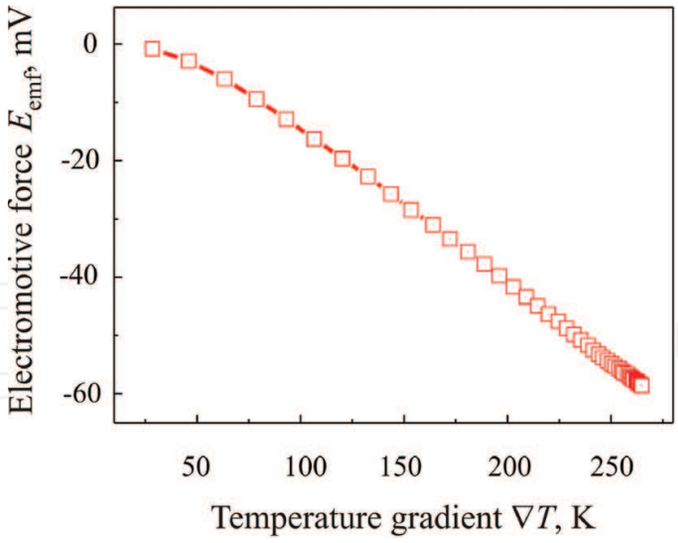

Figure 6. Electromotive force E_{emf} dependence upon the temperature gradient for PdO film prepared by oxidation at T_{ox} = 870 K (thickness ~ 30 nm).

In view of *p*-type conductivity, palladium (II) oxide films are characterized with the cation deficiency regarding the stoichiometric 1:1 ratio. Thus, for PdO, the Kröger-Vink defect reactions can be written as follows:

a. with the cations in deficiency on the lattice sites:

$$Pd_{Pd}^{\times} + O_O^{\times} + \frac{1}{2}O_2^{(gas)} \rightleftarrows Pd_{Pd}^{\times} + V_{Pd}^{''} + 2\,O_O^{\times} + 2\,h^{\cdot\cdot} \tag{2}$$

b. with the anions in excess on the interstitial sites:

$$Pd_{Pd}^{\times} + O_O^{\times} + \frac{1}{2}O_2^{(gas)} \rightleftarrows Pd_{Pd}^{\times} + O_O^{\times} + O_i^{''} + 2\,h^{\cdot\cdot} \tag{3}$$

The results obtained in the present work correlate with the capacitance voltage characteristics of PdO films on silicon [49]. Previously it was found that within the band gap of PdO films, one single energy state is realized only [49]. Therefore, only one type of point defects, which have generated holes, dominates in palladium (II) oxide films. The experimental study of the point defects nature will be the subject of further investigations.

5. Gas sensor properties of palladium (II) oxide nanostructures

Ozone and nitrogen dioxide sensitivity has been measured using the specially fabricated test samples of gas sensors based on thin and ultrathin PdO films oxidized at T_{ox} = 870 K. During sensor response measurements of PdO, ultrathin and thin films prepared by oxidation at T_{ox} = 873 K, synthetic air, calibrated gas mixtures with fixed nitrogen dioxide concentration, and standardized ozone generator produced by Optec were used. The ozone gas was generated by

oxidizing oxygen molecules of synthetic air (SA) by a pen-ray ultraviolet (UV) lamp calibrated to give the O_3 concentration range between 0.03 ppb and 800 ppb. The synthetic air containing ozone was blown directly on the sensor placed on the top of holder within the test chamber. The operating temperature T_d of the sensor ranging from room temperature to 670 K was controlled by chromel-alumel thermocouple. The measurement started after the sample resistance achieved a steady value [50, 51].

Sensor response S was determined as the ratio of the sensor resistance in synthetic air R_0 to the sensor resistance in gas R:

$$S = \frac{R_0}{R} \tag{4}$$

The measurements of NO_2 and O_3 concentration were performed in flow path conditions with the rates of 300 cm^3 per minute and 2.4 dm^3 per minute, respectively. The gas flow rate was measured by controllers produced by Bronkhorst.

As it possible to see in **Figures 7** and **8**, at rather low operation temperature T_d, the sensors based on thin (T_d = 490 K) and ultrathin (T_d = 448 K) PdO films show good sensitivity to rather low concentrations of ozone. **Figures 7** and **8** show that at process of ozone quantitative detection at SA atmosphere within concentration interval 100–250 ppb, palladium (II) oxide films have demonstrated high values of sensor response, signal stability, and reproducibility of sensor response also. This fact was proved by the results of multiple measurement cycles with the same O_3 concentrations. PdO films with thickness of about 35 nm are characterized by higher values of sensor response (on the average in 7–8 times) in comparison with ultrathin films at the same ozone concentrations (**Figure 9**). It is possible to explain

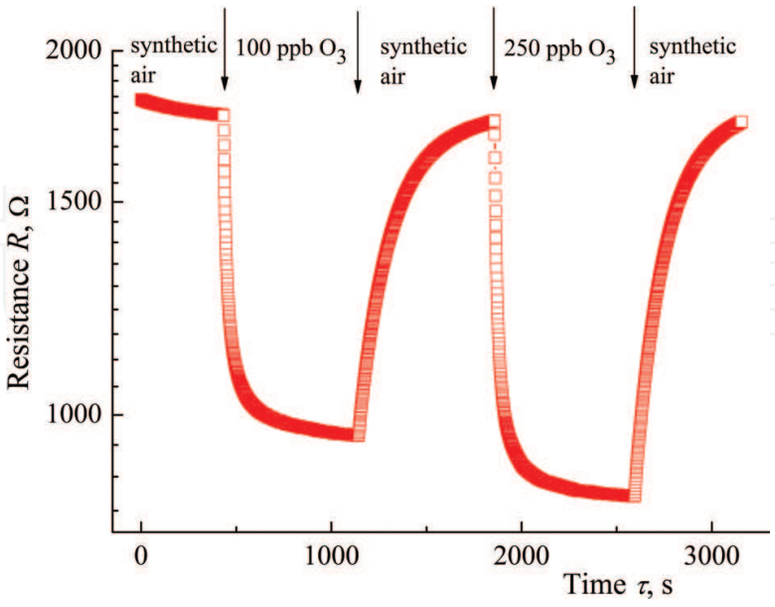

Figure 7. Time dependence of PdO ultrathin film (thickness ~ 10 nm) sensor resistance R at ozone different concentrations (operation temperature T_d = 448 K).

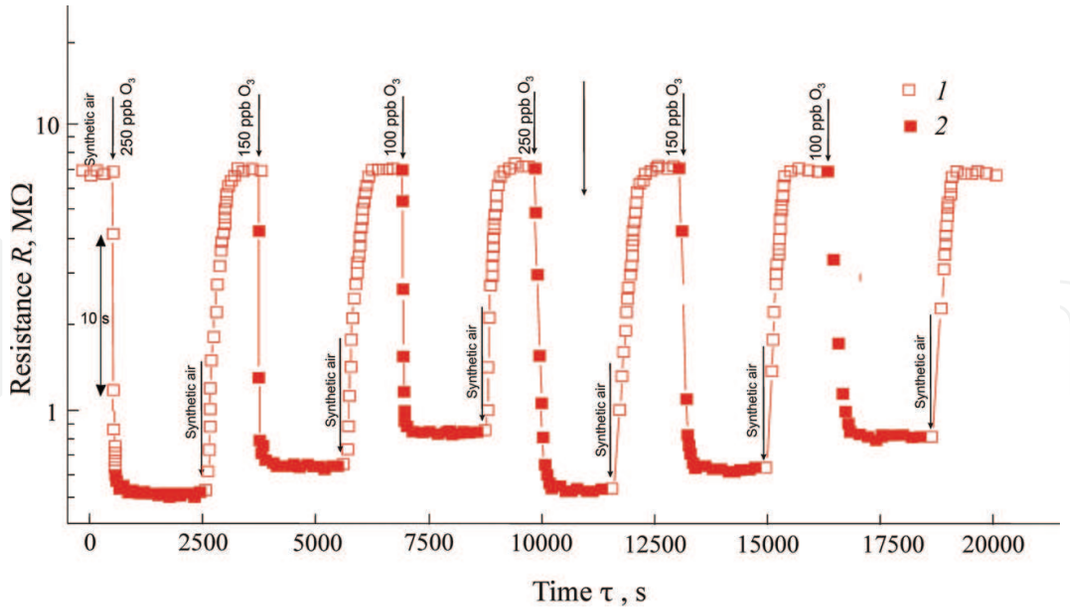

Figure 8. Time dependence of PdO thin film (thickness ~ 35 nm) sensor resistance *R* at ozone different concentrations (operation temperature T_d = 490 K).

this fact that the contribution in integrated conductivity of near-surface layers with high defects density is essentially higher for ultrathin PdO films than for films with thickness of about 35 nm (**Figure 9**). It is necessary to emphasis that the established feature demands a detailed study.

It has been established that PdO thin and ultrathin film sensors gave the stable signal, and the resistance values reliably returned to the baseline at SA atmosphere [50, 51]. It is necessary to note that the recovery period is quite long (600–700 s). It is necessary to note that the similar sensor behavior is typical for other materials used oxidizing gas detection. Usually in this case, the long recovery period is explained by the absence of oxidizing gas immediate interaction with oxygen molecules adsorbed on sensor material surface. At reducing gas detection, the direct interaction with oxygen molecules takes place; therefore, the recovery time is quite short. Moreover, the recovery time depends significantly on the operating temperature.

The sensitivity of palladium (II) oxide ultrathin films to nitrogen dioxide (another toxic oxidizing gas) has also been tested (**Figure 10**). As it can be seen in **Figure 10**, at the process of NO_2 quantitative detection within concentration interval 500 ppb–200 ppm, PdO ultrathin films have demonstrated good values of sensor response, signal stability, and reproducibility of sensor response [51]. It is necessary to note that the recovery period at NO_2 detection is longer than that at O_3 detection (**Figures 7**, **8**, and **10**).

During the determination of ozone (concentration φ = 100 ppb) and nitrogen dioxide (concentration φ = 10 ppm), the temperature dependences of PdO ultrathin film sensor response *S* are presented in **Figure 11**.

It is found that within interval of operation temperature 323 < T_d < 623 K, the maximum values of response *S* have been observed at T_d = 448 K (NO_2 detection) and at T_d = 490 K (O_3 detection).

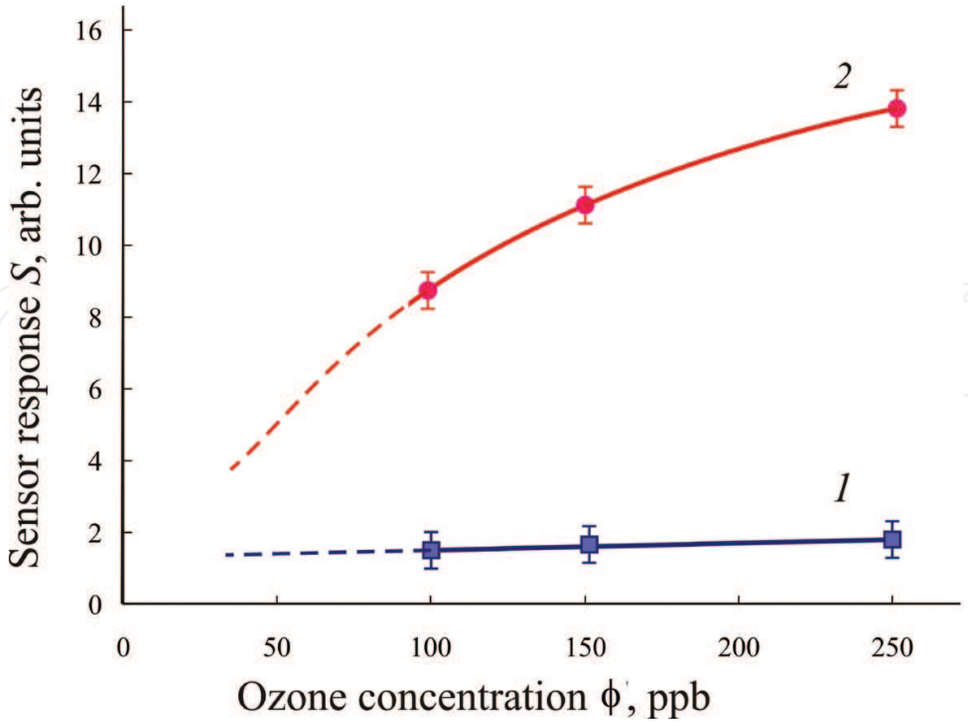

Figure 9. Dependence of PdO ultrathin and thin film sensor response *S* at ozone different concentrations: 1—Ultrathin film (thickness ~ 10 nm, operation temperature T_d = 448 K) and 2—Thin film (thickness ~ 35 nm, operation temperature T_d = 490 K).

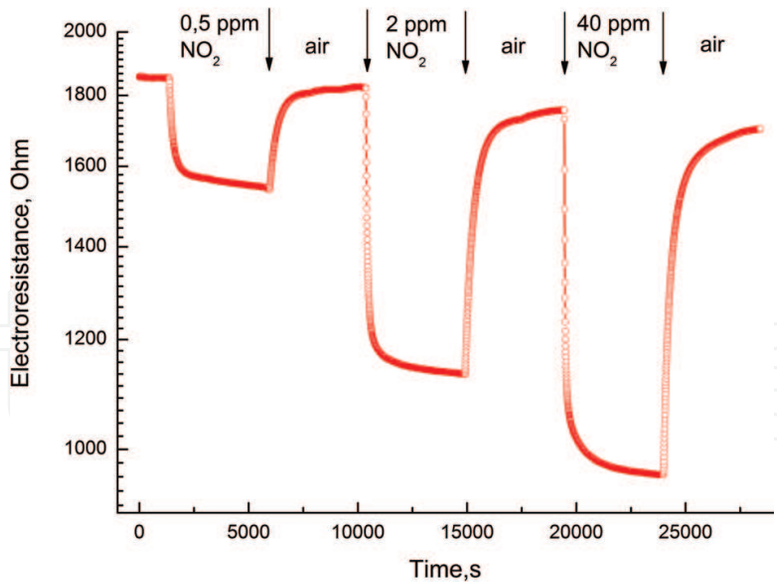

Figure 10. Time dependence of PdO ultrathin film (thickness ~ 10 nm) sensor resistance *R* at nitrogen dioxide different concentrations (operation temperature T_d = 448 K).

As it can be seen in **Figure 11**, approximately equal values of sensor response *S* of palladium (II) oxide films are realized at different concentration of oxidizing gases: $\phi(O_3)$ = 0.1 ppm and $\phi(NO_2)$ = 10 ppm.

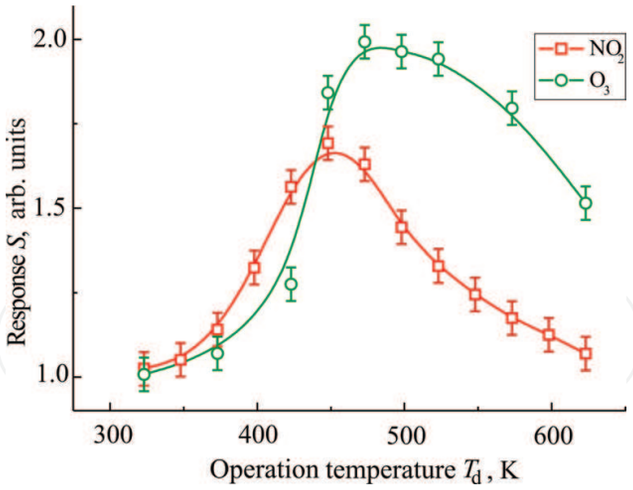

Figure 11. Dependence of PdO ultrathin film (thickness ~ 10 nm) sensor response S upon the operation temperature T_d at detection of ozone (O_3 concentration 0.1 ppm) and nitrogen dioxide (NO_2 concentration 10 ppm).

6. Discussion

Data presented in **Table 2** show that physical properties (molecular mass, electric dipole moment) and chemical properties (structure of molecule, high oxidative activity) of detected gases are very similar. According to experimental evidence from microwave spectroscopy, ozone and nitrogen dioxide are bent molecules with C_{2v} symmetry (**Table 2**). O_3 and NO_2 are the polar molecules with a dipole moment of 0.66 and 0.39 D, respectively.

Data in **Table 2** show that ozone and nitrogen dioxide molecules essentially differ with magnetic properties only. Ozone is diamagnetic, which means that its electrons are all paired. Unlike ozone, the ground electronic state of nitrogen dioxide is a doublet state. Owing to since nitrogen atom has one unpaired electron NO_2 molecule is paramagnetic.

Nevertheless, at detection of ozone and nitrogen dioxide, the temperature that has matched the maximum values of sensor response differs only 25°. Thus, there is prerequisite for the increase in selectivity of palladium (II) oxide sensors at O_3 and NO_2 detection after studying in detail that oxidation procedure conditions influence on microstructure and stoichiometry deviation.

Moreover, at ambient conditions, palladium (II) oxide is insoluble in water and does not react with it. As the bottom sediment, the palladium (II) hydroxide is formed only at interaction of soluble palladium (II) salt and alkali [52]. These facts are favorable for fabrication of gas detectors because they make possible to minimize the air humidity influence on PdO sensor response values.

To estimate such perspective for palladium (II) oxide nanostructures, we have allowed the speculative extrapolation of experimental data to the point that corresponds to zero ozone concentration (**Figure 12**). At ozone concentration ϕ = 10 ppb, which corresponds to 0.1 × PEL (permissible exposure limit), sensor response S would be about 2 (S ~ 2 is an open circle in **Figure 12**). The extrapolated sensitivity value at concentration $\phi(O_3)$ = 0.1 × PEL arouses hope that palladium (II) oxide films will be used in fabrication of ozone sensors.

At interaction with PdO surface ozone molecules are more active than nitrogen dioxide ones. This interaction is accompanied by more essential increase in the hole density of palladium (II) oxide ultrathin films. In general case, the surface interaction of PdO nanostructures can be written within the framework of Kröger-Vink notation:

$$Pd_{Pd}^{\times} + O_O^{\times} + O_3^{(gas)} \rightleftarrows Pd_{Pd}^{\times} + O_O^{\times} + O_i'' + 2h^{\cdot\cdot} + O_2^{(gas)} \quad (5)$$

According to Eq. (5), oxygen atom is integrated with palladium (II) oxide structure and O_2 molecule is desorbed from the surface. As result of this reaction (5), two holes are formed.

From this point of view, it is possible to explain high efficiency of palladium (II) oxide films at ozone detection. The attempt to distinguish the real reason of PdO nanostructures' higher

Molecule	Molar mass M, g × mol^{-1}	Space group symmetry	Magnetic Properties	Magnetic susceptibility $\chi \times 10^6$, cm^3/mol	Dipole moment $\mu \times 10^{30}$, C·m	PEL, ppm
O_3	48.00	C_{2v}	Diamagnetic	+6.7	2.2	0.1
					0.66D	(0.2 mg/m3)
NO_2	46.0055	C_{2v}	Paramagnetic	+150.0	1.3	5
					0.39D	(9 mg/m3)

Table 2. Physicochemical properties and permissible exposure limit (PEL) of ozone and nitrogen dioxide [52–56].

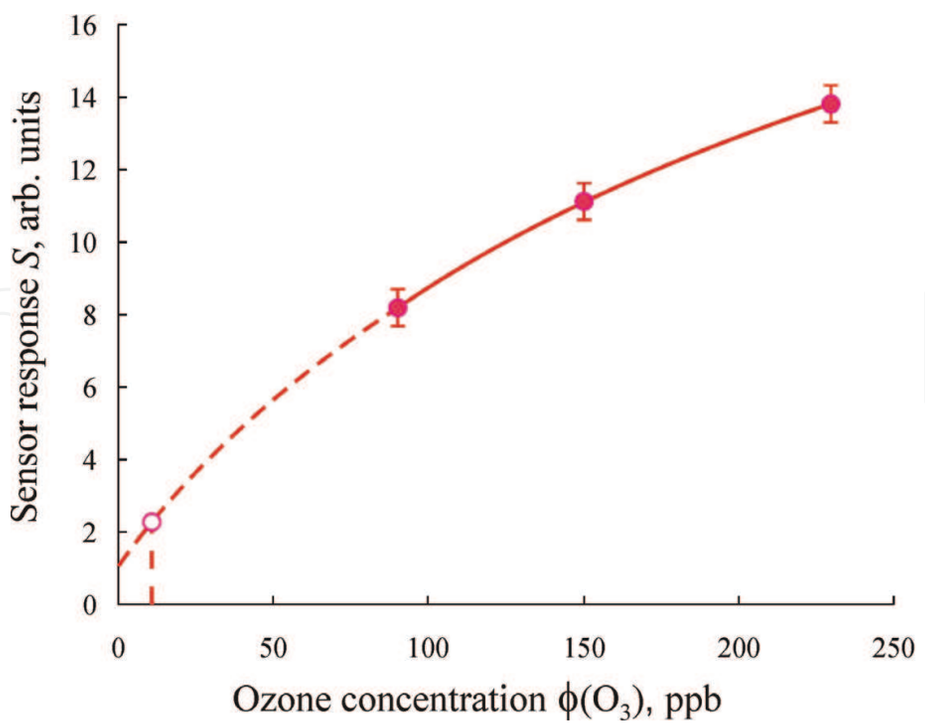

Figure 12. Dependence of PdO sensor response *S* upon the ozone concentration in synthetic air (operating temperature T_d = 490 K (220°C).

sensitivity to ozone, it should be looked for ozone's extremely high oxidizing ability. As it can be seen in **Table 2**, the PEL value of ozone is smaller than the similar characteristic of nitrogen dioxide by 50 times practically. This fact is the indirect evidence of ozone-exclusive oxidizing activity. The difference in sensitivity of palladium (II) oxide nanostructures at ozone and nitrogen dioxide detection will be a subject of the subsequent experiments and discussions. Now, it is possible to designate the direction of these future researches only. It is reasonable to assume that under ozone molecules impact, the metastable nanoclusters are formed on the surface of PdO, in which the oxidation states of palladium are higher than (II), for example, (III) or (IV).

7. Conclusion

The results of X-ray analysis, HEED, and HR TEM have demonstrated the possibility of the synthesis of homogeneous nanocrystalline thin and ultrathin films of palladium (II) oxide on different substrates. The very first examinations of sensitivity to different nitrogen dioxide and ozone concentration at rather low operating temperature have shown the high values of sensor response, signal stability, operation speed, and reproducibility of PdO films sensor response. The possibility of work at quite low temperatures will allow decreasing in the energy consumption of the analytical instruments. The detection of O_3 and NO_2 by palladium (II) oxide sensors can be applied in the fields of the human health and environment protection. Because the synthesis procedure is rather simple and compatible with planar processes of the microelectronic industry PdO nanostructures have a good perspective to be one of the main materials for commercial fabrication of oxidizing gases (ozone, nitrogen dioxide, chlorine etc.) sensors.

Author details

Alexander M. Samoylov[1]*, Stanislav V. Ryabtsev[1], Vasily N. Popov[1] and Petre Badica[2]

*Address all correspondence to: samoylov@chem.vsu.ru

1 Voronezh State University, Universitetskaya, Voronezh, Russian Federation

2 National Institute of Materials Physics, Atomistilor, Magurele, Ilfov, Romania

References

[1] Estimating Mortality Risk Reduction and Economic Benefits from Controlling Ozone Air Pollution. Report of the US National Academies of Sciences. Washington: The National Academies Press; 2008. 247 p

[2] Health Aspects of Air Pollution with Particulate Matter, Ozone and Nitrogen Dioxide. Report on a WHO Working Group, 13-15-01-2003. Bonn, Germany: ©World Health Organization. 2003. 94 p

[3] Amos P. K. Tai, Maria Val Martin, Colette L. Heald. Threat to future global food security from climate change and ozone air pollution. Nature Climate Change. Letters. Published online: 27-07-2014. DOI:10.1038/nclimate2317

[4] Chandra Kala, Syed Salman Ali, Abid Mohd, Sweety Rajpoot, Najam Ali Khan. Protection against fca induced oxidative stress induced dna damage as a model of arthritis and in vitro anti-arthritic potential of *Costus speciosus* rhizome extract. International Journal of Pharmacognosy and Phytochemical Research. 2015;**7**(2):383-389

[5] Parellada M, Moreno C, Mac-Dowell K, Leza JC, Giraldez M, Bailón C, Castro C, Miranda-Azpiazu P, Fraguas D, Arango C. Plasma antioxidant capacity is reduced in Asperger syndrome. Journal of Psychiatric Research. 2012;**46**:394-401

[6] Joseph N, Zhang-James Y, Perl A, Faraone SV. Oxidative stress and ADHD: A meta-analysis. Journal of Attention Disorders. 2015;**19**:915-924

[7] Hwang O. Role of oxidative stress in Parkinson's disease. Experimental Neurology. 2013;**22**:11-17

[8] Giacco F, Brownlee M. Oxidative stress and diabetic complications. Circulation Research. 2010;**107**(9):1058-1070

[9] Romá-Mateo C, Aguado C, García-Giménez JL, Ibáñez-Cabellos JS, Seco-Cervera M, Pallardó FV, Knecht E, Sanz P. Increased oxidative stress and impaired antioxidant response in lafora disease. Molecular Neurobiology. 2015;**51**:932-946

[10] Popov VN. Possible role of free oxidation processes in the regulation of reactive oxygen species production in plant mitochondria. Biochemical Society Transactions. 2003;**31**, part 6:1316-1317

[11] Shiri Avnery, Denise L. Mauzerall, Junfeng Liu, Larry W. Horowitz. Global crop yield reductions due to surface ozone exposure: 1. Year 2000 crop production losses and economic damage. Atmospheric Environment. 2011;**45**:2284-2296

[12] Avnery S, Mauzerall DL, Liu J, Horowitz LW. Global crop yield reductions due to surface ozone exposure: 2. Year 2030 potential crop production losses and economic damage under two scenarios of O_3 pollution. Atmospheric Environment. 2011;**45**:2297-2309

[13] Popov VN. Feedback loop of non-coupled respiration and reactive oxygen species production in plant mitochondria. In: Kapuganti Jagadis Gupta and Abir U. Igamberdiev. Reactive Oxygen and Nitrogen Species Signaling and Communication in Plants. Vol. 23., ed. Switzerland: ©Springer International Publishing; 2015. 316 p

[14] Krivetskiy V, Ponzoni A, Comini E, Badalyan S, Rumyantseva M, Gaskov A. Selectivity modification of SnO_2-based materials for gas sensor arrays. Electroanalysis. 2010;**22**:1-8

[15] Badalyan SM, Rumyantseva MN, Nikolaev SA, Marikutsa AV, Smirnov VV, Alikhanian AS, Gaskov AM. Effect of au and NiO catalysts on the NO_2 sensing properties of nanocrystalline SnO_2. Inorganic Materials. 2010;**46**:232-236

[16] Jung S-H, Choi S-W, Kim SS. Fabrication and properties of trench-structured networked SnO_2 nanowire gas sensors. Sensors and Actuators B. 2012;**171-172**:672-678

[17] Oros C, Horprathumb M, Wisitsoraat A, Srichaiyaperk T, Samransuksamer B, Limwichean S, Eiamchai P, Phokharatkul D, Nuntawong N, Chananonnawathorn C, Patthanasettakul V, Klamchuen A, Kaewkhaoe J, Tuantranont A, Chindaudom P. Ultra-sensitive NO_2 sensor based on vertically aligned SnO_2 nanorods deposited by DC reactive magnetron sputtering with glancing angle deposition technique. Sensors and Actuators B. 2016;**223**:936-945

[18] Adelina Stanoiu, Simona Somacescu, Jose Maria Calderon-Moreno,Valentin Serban Teodorescu, Ovidiu Gabriel Florea, André Sackmann, Cristian Eugen Simion. Low level NO_2 detection under humid background and associated sensing mechanism for meso-porous SnO_2, Sensors and Actuators B. 2016;**231**:166-174

[19] Zhao X, Shi W, Mu H, Xie H, Liu F. Templated bicontinuous tin oxide thin film fabrication and the NO_2 gas sensing. Journal of Alloys and Compounds. 2016;**659**:60-65

[20] Yuling Wei, Changlong Chen, Guangzheng Yuan, Shuai Gao. SnO_2 nanocrystals with abundant oxygen vacancies: Preparation and room temperature NO_2 sensing. Journal of Alloys and Compounds. 2016;**681**:43-49

[21] Saboor FH, Ueda T, Kamada K, Hyodo T, Mortazavi Y, Khodadadi AA, Shimizu Y. Enhanced NO_2 gas sensing performance of bare and Pd-loaded SnO_2 thick film sensors under UV-light irradiation at room temperature. Sensors and Actuators B. 2016;**223**:429-439

[22] Jiao M, Chien NV, Duy NV, Hoa ND, Van Hieu N, Hjort K, Nguyen H. On-chip hydrothermal growth of ZnO nanorods at low temperature for highly selective NO_2 gas sensor. Materials Letters. 2016;**169**:231-235

[23] Katoch A, Sun G-J, Choi S-W, Byun J-H, Kim SS. Competitive influence of grain size and crystallinity on gas sensing performances of ZnO nanofibers. Sensors and Actuators B. 2013;**185**:411-416

[24] Lontio Fomekong R, Lahem D, Debliquy M, Yunus S, Lambi Ngolui J, Delcorte A. $Ni_{0.9}Zn_{0.1}O$/ZnO nanocomposite prepared by malonate coprecipitation route for gas sensing. Sensors and Actuators B. 2016;**231**:520-528

[25] Lingmin Y, Guo F, Liu S, Yang B, Jiang Y, Qi L, Fan X. Both oxygen vacancies defects and porosity facilitated NO_2 gas sensing response in 2D ZnO nanowalls at room temperature. Journal of Alloys and Compounds. 2016;**682**:352-356

[26] Ganbavle VV, Inamdar SI, Agawane GL, Kim JH, Rajpure KY. Synthesis of fast response, highly sensitive and selective Ni:ZnO based NO_2 sensor. Chemical Engineering Journal. 2016;**286**:36-47

[27] Jaina R, Leib Y, Maric R. Ultra-low NO_2 detection by gamma WO_3 synthesized by reactivespray deposition technology. Sensors and Actuators B. 2016;**236**:163-172

[28] Van PTH, Do DD, Duy NV, Hoa ND, Hieu NV. Ultrasensitive NO_2 gas sensors using tungsten oxide nanowires with multiple junctions self-assembled on discrete catalyst islands via on-chip fabrication. Sensors and Actuators B. 2016;**227**:198-203

[29] Hi Gyu Moon, Soo Deok Han, Min-Gyu Kang, Woo-Suk Jung, Beomjin Kwon,Chulki Kim, Taikjin Lee, Seok Lee, Seoung-Hyub Baek, Jin-Sang Kim, Hyung-Ho Park, Chong-Yun Kang. Glancing angle deposited WO_3 nanostructures for enhanced sensitivity and selectivity to NO_2 in gas mixture. Sensors and Actuators B. 2016;**229**:92-99

[30] Kim J-S, Yoon J-W, Hong YJ, Kang YC, Abdel-Hady F, Wazzan AA, Lee J-H. Highly sensitive and selective detection of ppb-level NO_2 using multi-shelled WO_3 yolk–shell spheres. Sensors and Actuators B. 2016;**229**:561-569

[31] Giancaterini L, Emamjomeh SM, De Marcellis A, Palange E, Resmini A, Anselmi-Tamburini U, Cantalini C. The influence of thermal and visible light activation modes on the NO_2 response of WO_3 nanofibers prepared by electrospinning. Sensors and Actuators B. 2016;**229**:387-395

[32] Zhang W, Ming H, Liu X, Wei Y, Na L, Qin Y. Synthesis of the cactus-like silicon nanowires/tungsten oxide nanowires composite for room-temperature NO_2 gas sensor. Journal of Alloys and Compounds. 2016;**679**:391-399

[33] Ilin A, Martyshov M, Forsh E, Forsh P, Rumyantseva M, Abakumov A, Gaskov A, Kashkarov P. UV effect on NO_2 sensing properties of nanocrystalline In_2O_3. Sensors and Actuators B. 2016;**231**:491-496

[34] Xiao B, Wang F, Zhai C, Wang P, Xiao C, Zhang M. Facile synthesis of In_2O_3 nanoparticles for sensing properties at low detection temperature. Sensors and Actuators B. 2016;**235**:251-257

[35] Navale ST, Tehare KK, Shaikh SF, Patil VB, Pawar BN, Naushad M, Stadler FJ, Mane RS. Hexamethylenetetramine-mediated TiO_2 films: Facile chemical synthesis strategy and their use in nitrogen dioxide detection. Materials Letters. 2016;**173**:9-12

[36] Rey E, Kamal MR, Miles RB, Royce BSH. The semiconductivity and stability of palladium oxide. Journal of Materials Science. 1978;**13**:812-816

[37] Nilsson PO, Shivaraman MS. Optical properties of PdO in the range of 0.5-5.4 eV. Journal of Physics C: Solid State Physics. 1979;**12**:1423-1427

[38] Ryabtsev SV, Shaposhnik AV, Samoylov AM, Sinelnikov AA, Soldatenko SA, Kuschev SB, Ievlev VM. Thin films of palladium oxide for gas sensors. Doklady Physical Chemistry. 2016;**470**:158-161

[39] Kneer J, Wöllenstein J, Palzer S. Manipulating the gas–surface interaction between copper (II) oxide and mono-nitrogen oxides using temperature. Sensors and Actuators B. 2016;**229**:57-62

[40] Kim J-H, Katoch A, Choi S-W, Kim SS. Growth and sensing properties of networked p-CuO nanowires. Sensors and Actuators B. 2015;**212**:190-195

[41] Yamazoe N, Kurokawa Y, Seiyama T. Effects of additives on semiconductor gas sensors. Sensors and Actuators B. 1983;**4**:283-289

[42] Ievlev VM, Kushchev SB, Sinel'nikov AA, Soldatenko SA, Ryabtsev SV, Bosykh MA, Samoilov AM. Structure of heterosystems formed by a SnO_2 film and island metal (Ag, au, or Pd) condensate. Inorganic Materials. 2016;**52**:700-707. DOI: 10.1134/S0020168516070062

[43] Marikutsa AV, Rumyantseva MN, Gaskov AM, Samoylov AM. Nanocrystalline tin dioxide: Basics in relation with gas sensing phenomena. Part II. Active Centers and Sensor Behavior, Inorganic Materials. 2016;**52**:1327-1354

[44] Korotcenkov G, Cho BK. Ozone measuring: What can limit application of SnO_2-based conductometric gas sensors? Sensors and Actuators B. 2012;**161**:28-44. DOI: 10.1016/j.snb.2011.12.003

[45] Marikutsa AV, Rumyantseva MN, Gaskov AM, Samoylov AM. Nanocrystalline tin dioxide: Basics in relation with gas sensing phenomena. Part I. Physical and chemical properties and sensor signal formation. Inorganic Materials. 2015;**51**:1329-1347. DOI: 10.1134/S002016851513004X

[46] Ievlev VM, Ryabtsev SV, Shaposhnik AV, Samoylov AM, Kuschev SB, Sinelnikov AA. Ultrathin films of palladium oxide for oxidizing gases detecting. Procedia Engineering. 2016;**168**:1106-1109

[47] Samoylov A, Ryabtsev S, Shaposhnik A, Kuschev S, Soldatenko S, Ievlev V. Palladium oxide thin film for oxidizing gases detecting. The 16-th International Meeting on Chemical Sensors IMCS 2016. Final Program & Absrtacts Book: Jeju, Jeju Island, Korea, July 10-13; 2016. 96 p

[48] Ryabtsev SV, lyevlev VM, Samoylov AM, Kuschev SB, Soldatenko SA. Real microstructure and electrical properties of palladium oxide thin films for oxidizing gases detecting. Science and Application of Thin Films, Conference & Exhibition (SATF-2016). Çeşme, Izmir, Turkey, September 19-23: Book of Abstracts; 2016. 44 p

[49] Sobolev VV, Mordas DO, Sobolev VV. Optical properties and electronic structure of PdO. Inorganic Materials. 2004;**40**:166-170

[50] Ryabtsev SV, Ievlev VM, Samoylov AM, Kuschev SB, Soldatenko SA. Microstructure and electrical properties of palladium oxide thin films for oxidizing gases detection. Thin Solid Films. 2017;**636**:751-759

[51] Ievlev VM, Ryabtsev SV, Samoylov AM, Shaposhnik AV, Kuschev SB, Sinelnikov AA. Thin and ultrathin films of palladium oxide for oxidizing gases detection. Sensors & Actuators: B. Chemical Part 2. 2018;**255**:1335-1342

[52] Greenwood NN, Earnshaw A. Chemistry of the Elements. 2nd ed. Oxford: Butterworth-Heinemann; 1997. 1340 p

[53] Hodgeson JA, Sibert EE, Curl RF Jr. Dipole moment of nitrogen dioxide. Journal of Physical Chemistry. 1963;**67**(12):2833-2835. DOI: 10.1021/j100806a079

[54] Boggs JE. The dipole moments and polarizabilities of nitrogen dioxide and nitrogen tetroxide. Journal of Physical Chemistry. 1964;**68**(8):2379-2381. DOI: 10.1021/j100790a513

[55] The National Institute for Occupational Safety and Health (NIOSH). NIOSH Pocket Guide to Chemical Hazards. https://www.cdc.gov/niosh/npg/npgd0454.html

[56] General Chemistry Is A Free Introductory Textbook On Chemistry. http://www.vias.org/genchem/index.html

IntechOpen

IntechOpen